https://doi.org/10.5194/wes-2025-108
Preprint. Discussion started: 27 June 2025

eawe european academy of wind energy
Open Access WIND ENERGY SCIENCE DISCUSSIONS

Characterization of HRRR simulated Rotor Layer Wind Speeds and Clouds along Coast of California

Jungmin Lee[1], Virendra P. Ghate[2], Arka Mitra[2], Lee M. Miller[3], Raghavendra Krishnamurthy[3], and Ulrike Egerer[4]

[1]Lawrence Livermore National Laboratory, Livermore, CA 94550, USA
[2]Argonne National Laboratory, Lemont, IL 60439, USA
[3]Pacific Northwest National Laboratory, Richland, WA 99354, USA
[4]National Renewable Energy Laboratory, Golden, CO 80401, USA

Correspondence to: Jungmin Lee (lee1046@llnl.com)

Abstract. Stratocumulus clouds, with their low cloud base and top, affects the atmospheric boundary layer wind and turbulence profile, modulating wind energy resources. GOES satellite data reveals an abundance of stratocumulus clouds in late spring and summer months off the coast of Northern and Central California where there are active plans to deploy floating offshore wind farms at two lease areas (near Morro Bay and Humboldt). From fall 2020, two buoys with multiple instrumentations including lidar were deployed for about 1 year in these wind farm lease areas to assess the wind energy resources in these locations. In this study, we characterize the stratocumulus cloud properties and wind speed at turbine-relevant rotor layer (from surface to 300 m above sea level) in both buoy observations and the High Resolution Rapid Refresh (HRRR) model. First, we find that HRRR numerical model reproduces the seasonal cycle of cloud top height quite well in these locations. However, during the warm season, especially at Morro Bay, we find the stratocumulus clouds simulated by HRRR tend to have lower cloud tops by about 150 m and weaker diurnal cycles compared to the satellite reported cloud observations. Next, our findings show that the wind speed and vertical shear are stronger in Humboldt location than in Morro Bay. Also, those fields are stronger under clear sky conditions in both locations. Finally, our findings suggest that the model bias in rotor layer wind speed is small under cloudy conditions, while the bias is large and increases with observed wind speed under clear sky condition. At Morro Bay, the model under clear-sky condition is underestimating the observed wind speed, while at Humboldt, there is overestimation in the model simulated wind speed. The findings from this study will potentially inform how to improve the modeling of wind resources off the coast of Northern California.

1 Introduction

Due to the semi-permanent Pacific high-pressure system and cold sea surface temperatures (SST) from coastal upwelling, marine boundary layer clouds appear frequently off the coast of California year-round (Iacobellis et al., 2013, Lin et al., 2009). Especially during the warm season, marine stratocumulus and stratus (from here on, stratocumulus) are most pronounced. These clouds originate in subsiding dry and warm air as the high-pressure system interacts with the cold, humid,

https://doi.org/10.5194/wes-2025-108
Preprint. Discussion started: 27 June 2025

and shallow marine atmospheric boundary layer (MABL), forming a stronger capping inversion. This capping temperature and moisture inversion limits the vertical extent of the low-level clouds. Marine stratocumulus clouds are shallow (~200 m thickness) but optically thick, therefore inducing radiative cooling at the top of the boundary layer, primarily in the longwave spectrum. The cloud top radiative cooling along with surface buoyancy production, cloud top entrainment, and wind shear drive the turbulence in the MABL and hence the cloud and precipitation processes. As turbulence and cloud processes are intimately coupled in the MABL, the presence of marine stratocumulus affects the profile of winds and turbulent properties within the marine boundary layer (Wood 2012).

In July 2005, Marine Stratus/Stratocumulus Experiment (MASE) field campaign was carried out off the coast of Monterey (California) to sample the clouds and aerosols (Lu et al., 2007). Measurements including cloud base and top heights were made from a research flights 13 different times. Out of those measurements, cloud base height varied between 67 and 315 meters, and the cloud top height ranged from 268 to 732 meters. These measurements indicate that all or a lower portion of marine boundary layer clouds can exist in the wind turbine relevant height near the coast of California in summertime. Therefore, it is important to evaluate the influence of marine boundary layer clouds on the wind resources off the coast of California (Shaw et al., 2022).

Off the coast of California, there are active plans to deploy offshore wind farms at two lease areas, one along northern California near Humboldt Bay and another along central California near Morro Bay. Staring October 2020, Doppler lidar-equipped buoys that are owned by the US Department of Energy (DOE) were deployed to continuously measure the wind speed at various heights below 240-meter for one year (Krishnamurthy, 2023). This dataset provides a unique opportunity to evaluate the performance of numerical weather prediction (NWP) models at the planned wind farm locations. Sheridan et al. (2022) utilized this dataset to assess the bias in hub-height wind speed using various reanalysis and NWP model data. They also investigated potential relations between the bias in terms of atmospheric stability and shear strength. However, they did not consider the influence of MABL clouds as a source of model bias of the hub-height wind speed. Additionally, their analysis did not include an evaluation of winds simulated by the High-Resolution Rapid Refresh (HRRR) model, despite HRRR being one of the most widely utilized forecasting tools in wind energy resource assessments.

The aim of this study is to compare the modeled (HRRR) and observed (satellite and buoy) characteristics of stratocumulus clouds and winds at turbine relevant height and assess the HRRR bias in wind speed near the surface for better decision making in wind farm development off the coast of California. The paper is organized as follows: section 2 describes the brief description about the various datasets used in this study and how they were post-processed to allow direct comparisons. The characteristics of clouds, hub-height wind speed, and model wind bias in relation to of various cloud properties at Humboldt and Morro Bay locations are explored in Section 3. Summary and conclusion follow in Section 4.

https://doi.org/10.5194/wes-2025-108
Preprint. Discussion started: 27 June 2025

2 Data and Method

2.1 Lidar-buoy observation dataset

DOE-owned buoys with multiple instrumentations were deployed about 40-50 km off the coast of Morro Bay (35.71074◦ N, 121.84606◦ W) and Humboldt (40.9708◦ N, 124.5901◦ W). Each of the buoys started the operation in Fall of 2020 and the mission lasted about 1 year. In December 2020, a significant wave event at the Humboldt buoy location caused a power outage, resulting in a substantial data gap. The buoy equipment was restored and brought back online on May 25, 2021, at the Humboldt location. The details about the instruments on the buoys and methods for the raw data processing can be found in Krishnamurthy et al. (2023).

The buoys were equipped with WindCube 866 Doppler lidar to measure the vertical profiles of motion-compensated wind speed at 1 second temporal resolutions. The final post-processed wind profiles are at 10-minute temporal resolution with 10 m range resolution from from 40 to 240 meter above the surface.

The buoys were also equipped with LI-200SA pyranometer (PYR) to measure the global broadband solar radiation at 10-minute temporal frequency. By comparing the measured solar radiation to the modeled solar radiation for clear-sky conditions, we determined whether a cloud attenuated the downwelling solar radiation reaching to the surface (Long and Ackermann, 2000). Temporal cloud mask is estimated to be cloudy when the difference between the measured solar radiation and modeled clear sky solar radiation exceeds 10%, otherwise the condition is estimated to be cloud-free (Krishnamurthy et al., 2023).

2.2 Cloud top height from GOES

Cloud top heights over our study duration was taken from the SatCORPS Ed4 CERES-GOES record (Minnis et al. 2021). This record of ~8-km spatial resolution, hourly cloud property retrievals are prepared by the NASA Satellite ClOud and Radiation Property Retrieval System (SatCORPS) through the processing of GOES-15, GOES-16, and GOES-17 geostationary imagers belonging to the Geostationary Operational Environmental Satellite (GOES) program (Menzel and Purdom, 1994). These retrievals use the Clouds and the Earth's Radiant Energy System (CERES) Edition 4 (Ed4) algorithms, adapted for geostationary applications. These Ed4 algorithms and their nominal quality assessments can be found in Minnis et al. (2021). Since these retrievals from geostationary satellites are not provided over a fixed spatial grid, we prepared a time series of hourly retrievals that were closest to the buoy locations (Section 2.1). From here on, we shall simply refer to this record as GOES.

2.3 High Resolution Rapid Refresh (HRRR) v4

HRRR is a 3-km spatial resolution, hourly updating, convection permitting atmospheric forecast model developed and operated by National Oceanic and Atmospheric Administration (NOAA) (Dowell et al., 2022). HRRR specializes in providing short-term forecast with high fidelity, which particularly interests the wind energy community to better forecast wind power production. We use data from HRRRv4, which has been released in December 2020 and its data availability aligns

https://doi.org/10.5194/wes-2025-108
Preprint. Discussion started: 27 June 2025

eawe european academy of wind energy
Open Access WIND ENERGY SCIENCE DISCUSSIONS

with our buoy observation period. We utilize HRRR 3-hour forecast data that outputs wind speed at the native model vertical grid. By comparing the model's vertical grid with the lidar buoy's measurement height, we determine that the first 4 of the model's vertical height levels are close to the heights of the lidar measurement, which is at 40, 80, 160, and 240 meters. The HRRR reported wind profiles were linearly interpolated to get the wind speeds at 40, 80, 160, and 240 meters. We extract the data from the closest point to the buoy locations, which is not farther away than 1.5 km. We compute the wind speed bias by subtracting buoy reported wind speed from those reported by HRRR at 40, 80, 160, and 240 meter. Since HRRR provides hourly snapshots and the lidar buoy data represents 10-minute averages, we extract the corresponding lidar data for each hour to align with the HRRR time series.

3. Results

3.1 Characteristics of clouds off the coast of California

Figure 1(a,b) presents the distribution of cloud top heights computed by HRRR and estimated by GOES for each month of the observation period, and Figure 1 (c, d) show the same for cloud fraction. There are significant seasonal changes in cloud top heights and cloud fraction at both the Morro Bay and Humboldt locations. For Morro Bay, cloud fraction values from both HRRR and CERES exceed 80% consistently between May and September. In contrast, Humboldt Bay exhibits greater month-to-month variability in cloud fraction, with summer months not necessarily showing high values. The low cloud top heights (< 3 km) and high cloudiness between April and October, suggest the clouds to be low-level marine stratocumulus clouds. While higher cloud top heights (>7 km) and low cloudiness during the colder months suggest passage of mid-latitude frontal systems consistent with Lin et al., 2009. Overall, the winter months have higher cloud top heights than the summer months at both locations. This seasonal variation in cloud top height is accurately captured by the HRRR model. However, there are some minor discrepancies between the median values of observed and HRRR simulated cloud top heights. The quartile ranges and median values of cloud fraction reveal discrepancies between CERES and HRRR, with the differences being particularly pronounced for Humboldt Bay.

As we are interested in investigating the HRRR bias when low-altitude clouds interfere with the rotor layer, rest of the analysis only uses data from the warmer months. Guided by Fig. 1, the data from May through the end of September at both Morro Bay and Humboldt is composited. In December 2020, a large wave event at Humboldt buoy location results in the power outage and lead to a large data gap. The machines on the buoy were back online on May 25th, 2021, at Humboldt location. So, our results at the Humboldt location are missing most of May data.

https://doi.org/10.5194/wes-2025-108
Preprint. Discussion started: 27 June 2025

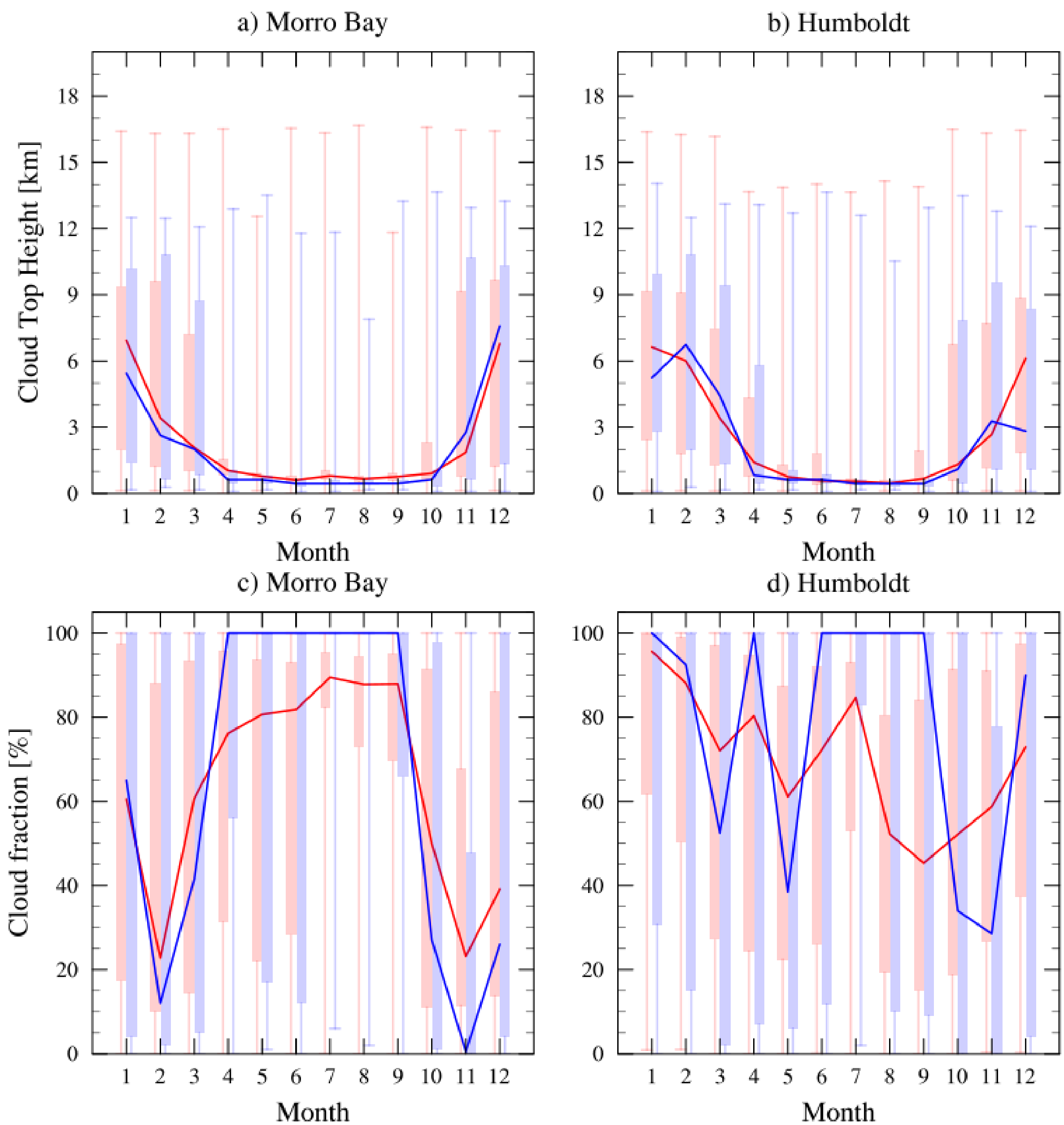

Figure 1 Box plot of (a, b) cloud top height from GOES (red) and HRRR (blue) and (c, d) cloud fraction from CERES (red) and HRRR (blue) for each month of the observation period at (left column) Morro Bay and (right column) Humboldt. The box represents 25th, and 75th percentile, and the bounding lines represent the minimum and maximum values. Median values are represented by thick lines.

Figure 2 shows the diurnal variation of MABL cloud top heights (cloud tops below 1.5 km) from HRRR and GOES over the warm season (May-Sept). On average, HRRR cloud tops are about 150 m lower than those in the GOES record at Morro Bay, while there is little difference at Humboldt location. The mean cloud top estimated by GOES is about 700 m at

https://doi.org/10.5194/wes-2025-108
Preprint. Discussion started: 27 June 2025

Morro Bay and 520 m at Humboldt, whereas HRRR estimates a mean cloud top height of around 550 m for both locations. A clear diurnal cycle in GOES cloud top height is present at both locations, which peaks around 10 AM local time (UTC - 8hr). The observed diurnal amplitude is larger for Morro Bay, while HRRR does not reproduce the diurnal cycle in both locations. The tops of stratocumulus clouds exhibit a distinct diurnal cycle, with higher values at night and lower values during the day, as cloud top radiative cooling is greater at night than during the daytime. The absence of a diurnal cycle in cloud top height in the HRRR model suggests an inaccurate representation of the diurnal cycle of cloud top radiative cooling-driven turbulence in the HRRR model.

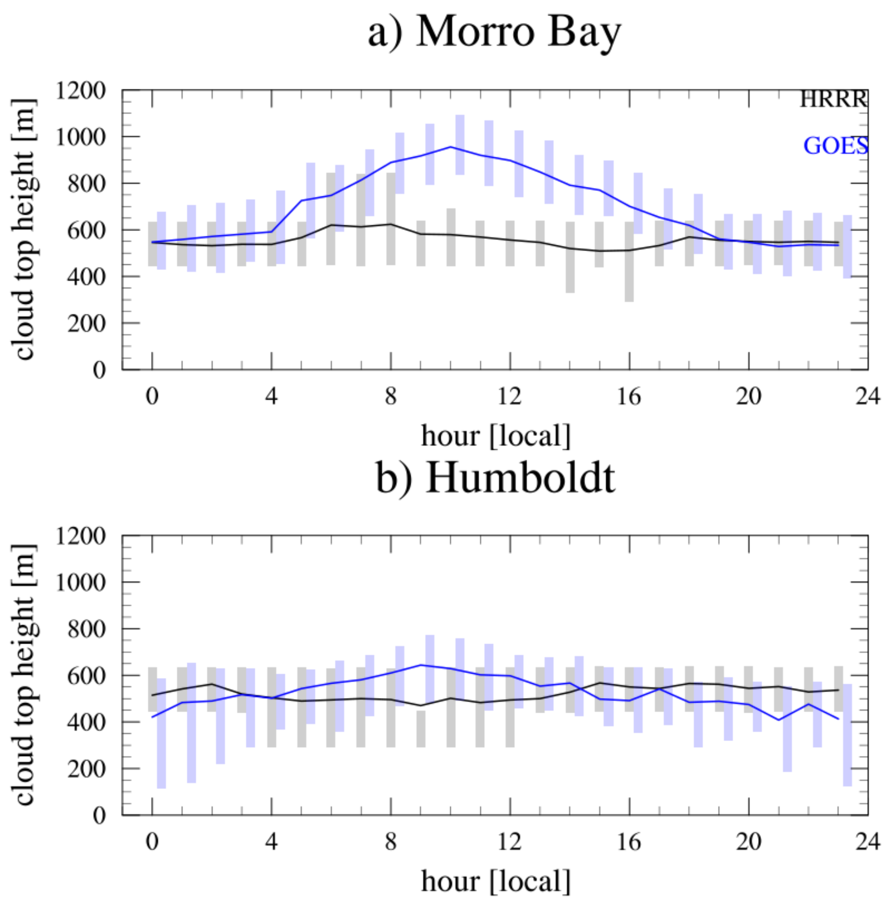

Figure 2 Warm season (May-Sept) diurnal cycle of cloud top height as reported by HRRR (gray) and GOES (blue) at (a) Morro Bay and (b) Humboldt Bay. Bounding boxes represent 25th and 75th percentile, while the lines represent the mean values.

Figure S1 shows the percentage of clear sky and cloudy sky days estimated by buoy, GOES, and HRRR between May-September at Morro Bay and Humboldt. For the buoy data, we utilize the estimated cloud mask, whereas for HRRR and GOES datasets, the cloud mask is derived from the percentage fraction of clouds, calculated as the proportion of all hours with valid cloud-top information. Out of 8,547 (11,951) buoy data samples collected at Morro Bay (Humboldt) during the warm season, 2,225 (4,529) were classified as clear-sky, while 6,322 (7,422) were classified as cloudy. Figure S1 indicates during

https://doi.org/10.5194/wes-2025-108
Preprint. Discussion started: 27 June 2025

warm season when the marine stratocumulus clouds are most pronounced, cloudy days are dominant off the coast of California and Morro Bay is cloudier than Humboldt, which is consistent with the finding in Krishnamurthy et al. (2023). HRRR-estimated cloud fraction slightly underestimates the buoy observed cloud fraction, which is less than 10 %, but is generally in good agreement with other sources of observation (GOES and buoy).

Throughout this study, we will investigate the HRRR bias in rotor layer wind speed in terms of cloudy days versus clear-sky days. Unless specified otherwise, only the warm season (May-Sept) data is considered in this study. Additionally, we are selecting a few case studies of marine stratocumulus clouds later in section 3.4 to investigate the model performance.

3.2 Variation of rotor layer wind speeds with cloudiness

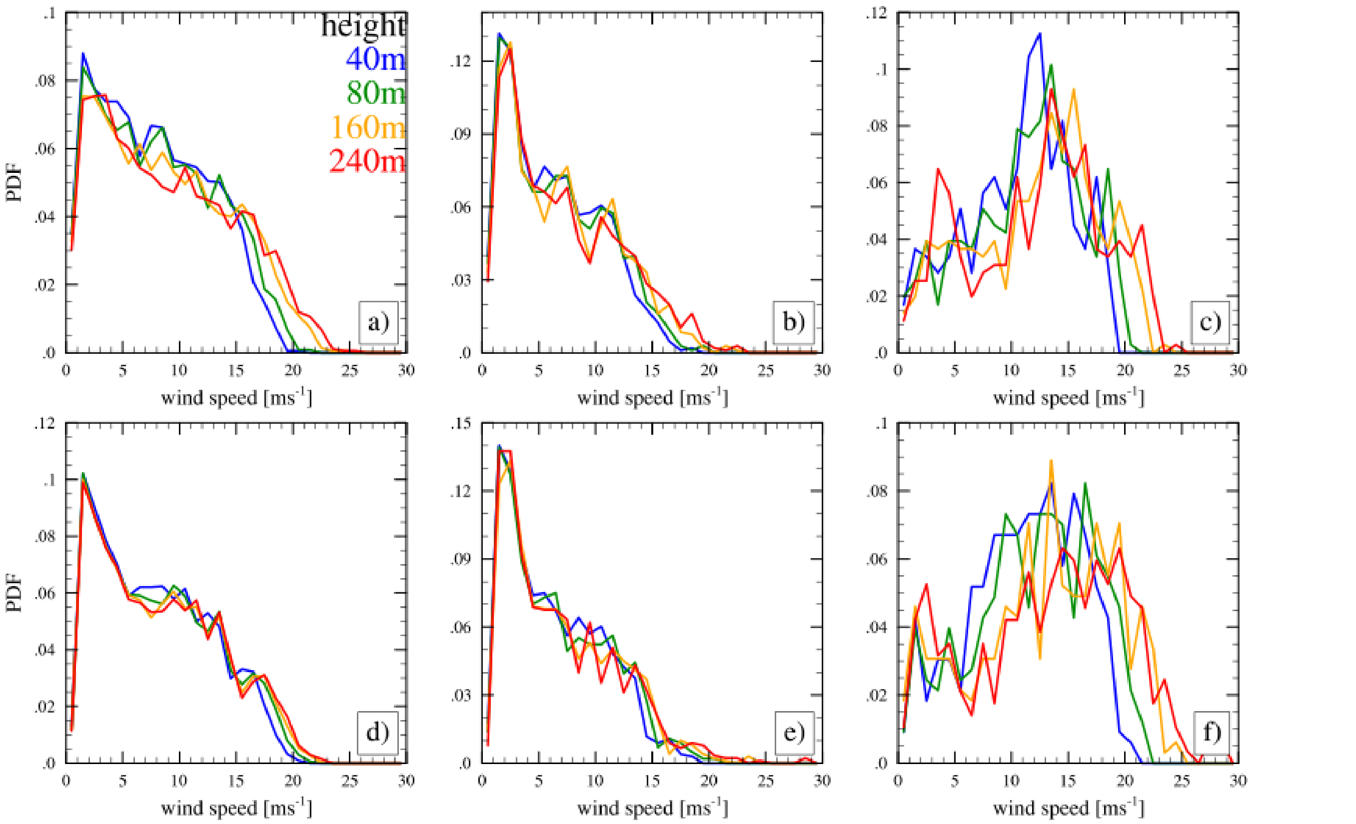

Figure 3 PDF of rotor layer (<= 240m) wind speed at Morro Bay from (top) HRRR, (bottom) lidar buoy during (left) all conditions, (middle column) cloudy conditions, and (right column) clear sky conditions.

In Fig. 3, we present the probability density function (PDF) distribution of wind speed at Morro Bay at 40, 80, 160, and 240 m heights from HRRR (a-c), and from the lidar buoy observation (d-f). We used the observed cloud mask from the buoys to distinguish between clear-sky and cloudy conditions. Rotor layer wind speeds from the lidar buoy at Morro Bay peaks around 1 - 2 m s^{-1} during cloudy condition, which is below typical cut-in speeds (3 – 4 m s^{-1}), while it peaks around 10 - 15 m s^{-1} during clear-sky conditions. Additionally, the peak of the PDF shifts towards higher wind speeds for clear-sky conditions

https://doi.org/10.5194/wes-2025-108
Preprint. Discussion started: 27 June 2025

and not for the cloudy conditions, suggesting presence of wind shear during the clear-sky conditions that is absent during cloudy conditions. This suggest that the turbulence is forced by wind shear during cloud-free conditions, while turbulence is only forced by cloud processes during cloudy conditions due to absence of shear. The rotor layer wind speed distributions at Morro Bay are well reproduced by HRRR model simulations with minor differences. During cloudy conditions, HRRR model does show a small increase in the wind speeds with height during cloudy conditions at higher wind speeds unlike the observations. During clear-sky conditions, the HRRR model did not simulate winds stronger than 25 m s^{-1}, that were reported on few instances by the lidar.

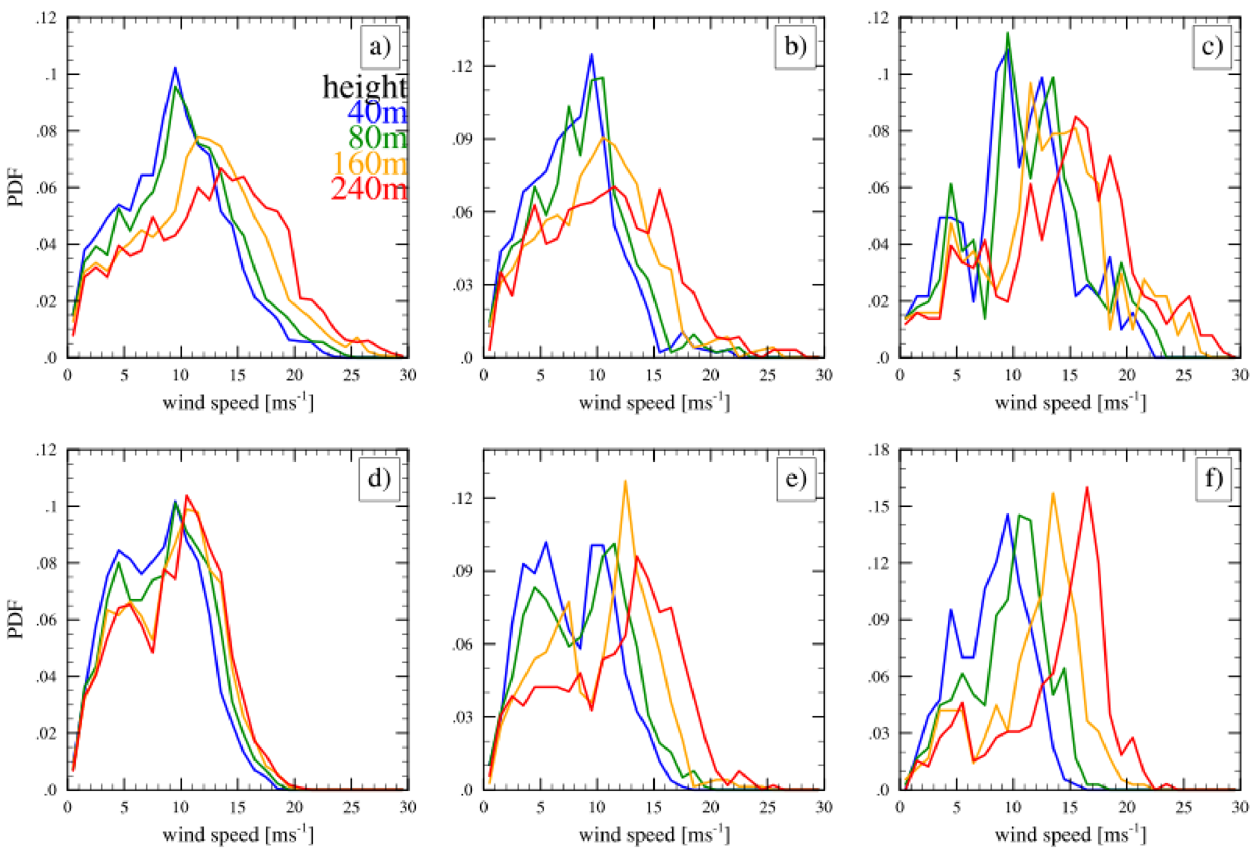

Figure 4 Same as Fig 3, but for Humboldt location.

In Fig. 4, we repeated the analysis shown in Fig. 3 for Humboldt Bay location. At Humboldt, the lidar buoy measurements of wind speed in the rotor layer shows a more spread-out distribution spanning 0 – 20 m s^{-1}, while HRRR reported winds range from 0 to 30 m s^{-1}. The HRRR model simulates a peak in the PDF (Figure 4a) that shifts toward higher speeds with increasing heights, unlike what is observed (Figure 4d). This suggests that HRRR model overestimates wind shear at Humboldt Bay location compared to the observations. At Humboldt, strong vertical shear is present regardless of cloud conditions, as the increase in wind speed with height is evident in both datasets, but HRRR model consistently overestimates

https://doi.org/10.5194/wes-2025-108
Preprint. Discussion started: 27 June 2025

this increase. During clear-sky conditions, the wind speed tends to be stronger compared to cloudy conditions, with peaks around 10 – 18 m s^{-1}. Collectively the figure suggests that at Humboldt Bay wind shear is forcing the turbulence during both cloudy and clear-sky conditions, with HRRR model overestimating the winds and the wind shear.

According to Table 1, mean 80-meter wind speed at Humboldt Bay is stronger than the one at Morro Bay regardless of weather conditions. The hub-height wind speed is stronger under clear-sky condition at both locations compared to that during cloudy conditions. We can relate clear-sky condition to stable stratification in atmospheric boundary layer. Under stable stratification, the surface layer—approximately 10% of the atmospheric boundary layer—becomes shallower in the marine boundary layer. This shallowness traps surface turbulent fluxes within the surface layer and decouples it from the layer above, leading to stronger wind speeds (Mahrt, 1999). These decoupled boundary layers are known to have lower cloudiness and higher winds than the coupled boundary layers (e.g. Serpetzoglou et al. 2008; Jones et al. 2011 etc.). The average wind speed difference between cloudy and clear-sky condition is stronger at Morro Bay, within both the buoy and HRRR records. During cloudy condition, HRRR is comparable to the observed hub-height wind speed. During clear sky condition, HRRR underestimates the hub-height wind speed at Morro Bay, while HRRR overpredicts it at Humboldt location.

Table 1 further demonstrates that the standard deviation of 80-meter wind speed during cloudy conditions is comparable between observations and HRRR at both locations. However, notable differences are observed under clear-sky conditions.

Table 1. Mean ± standard deviation of wind speed of the lidar buoy observation and HRRR at 80-meter height for cloudy and clear conditions.

	Observed		HRRR	
	Morro Bay [m s^{-1}]	Humboldt [m s^{-1}]	Morro Bay [m s^{-1}]	Humboldt [m s^{-1}]
Cloudy	6.7±4.4	8.5±4	6.6±4.3	8.5± 4
Clear	12±5.2	9.5±3.4	11.2±4.9	11.1±4.9

Following Wharton and Lundquist (2012), we compute the wind shear exponent α following:

$$\alpha = \frac{\ln{(v_2/v_1)}}{\ln{(z_2/z_1)}} \quad [1]$$

where v_2 is the wind velocity at height z_2 and v_1 is the wind velocity at height z_1. For this analysis we have set z_2=160 m and z_1 = 40 m. Table 2 lists α values using the lidar buoy observations and HRRR for Morro Bay and Humboldt under cloudy, and clear conditions. As mentioned earlier, α confirms that the shear is about 4 times stronger at Humboldt regardless of weather conditions. Stronger shear at Humboldt is also evident in the vertical profile of the lidar buoy wind speeds shown in Krishnamurthy et al. (2023). Under stable stratification, the surface layer is accompanied with weak turbulence, which lets stronger shear and veer to develop. Consistently, in both locations, shear is stronger under clear sky condition. The shear exponent is underestimated in HRRR at Humboldt location, while it is overestimated at Morro Bay. Previous modeling study

https://doi.org/10.5194/wes-2025-108
Preprint. Discussion started: 27 June 2025

by Zapata et al. (2021) showed that the cloud fraction decreases with an increase in near surface wind shear. Their results are consistent with our finding that cloud fraction in Humboldt (with stronger shear) is lower than in Morro Bay (Fig. 1).

Table 2. Mean ± standard deviation of wind shear exponent α of the lidar buoy observation and HRRR for cloudy and clear conditions.

	Observation		HRRR	
	Morro Bay	Humboldt	Morro Bay	Humboldt
Cloudy	0.05±0.10	0.2±0.22	0.07±0.13	0.15±0.14
Clear	0.07±0.22	0.26±0.16	0.09±0.13	0.16±0.15

3.3 Characteristics of hub-height wind speed bias in terms of cloudiness

Fig. 5 shows the distribution of 80-meter wind speed bias in HRRR, binned by observed wind speed. Prior to binning, data was separated by its weather conditions (i.e., total, cloudy, and clear-sky). The median difference between the observed and modeled winds is less than 1 m s^{-1} at both locations, while the range of the differences is higher at Morro Bay as compared to Humboldt Bay. At Morro Bay, the range of the bias across all observed wind speeds remains between ± 5 m s^{-1}, while this range is higher at the Humboldt Bay. At Morro Bay, HRRR model consistently underestimates the observed hub-height wind speed under cloudy condition with the underestimation increasing with an increase in the wind speed. During weak to moderate wind speed events (0 – 10 m s^{-1}) the HRRR model slightly overestimates the wind speed under clear-sky conditions, and then the bias sign changes as the observed wind speed is beyond 10 m s^{-1}. The change of the bias from positive to negative with increase in wind speed is the strongest under clear sky condition. The wind speed biases at Morro Bay during warm season are similar to those reported by Sheridan et al. (2022).

At Humboldt, HRRR slightly overestimates the hub-height wind speed when the observed wind speed is weak (0 – 5 m s^{-1}), regardless of weather conditions. However, unlike Morro Bay, median HRRR bias for hub-height wind speed under clear-sky condition remains positive even during strong wind speed events, while it changes to negative under cloudy condition. Similar to Morro Bay, the bias under clear-sky and cloudy conditions increases with higher observed wind speed. Because of the opposing bias signs between clear-sky and cloudy conditions at Humboldt, the median HRRR bias in hub-height wind speed over the entire period is close to zero. Our results are consistent with the findings in Sheridan et al. (2022), where the hub-height wind speed bias was investigated in terms of atmospheric stability. In Sheridan et al. (2022), the results by Rapid Refresh (RAP) indicated an overestimation of wind speed at Humboldt in stable conditions, while the bias flips its sign under unstable conditions. In their analysis, Morro Bay shows an underestimation of the wind speed regardless of the stability condition when RAP was compared to the lidar buoy observation. In both locations, the bias was much larger during the stable conditions, where the development of clouds is discouraged.

https://doi.org/10.5194/wes-2025-108
Preprint. Discussion started: 27 June 2025

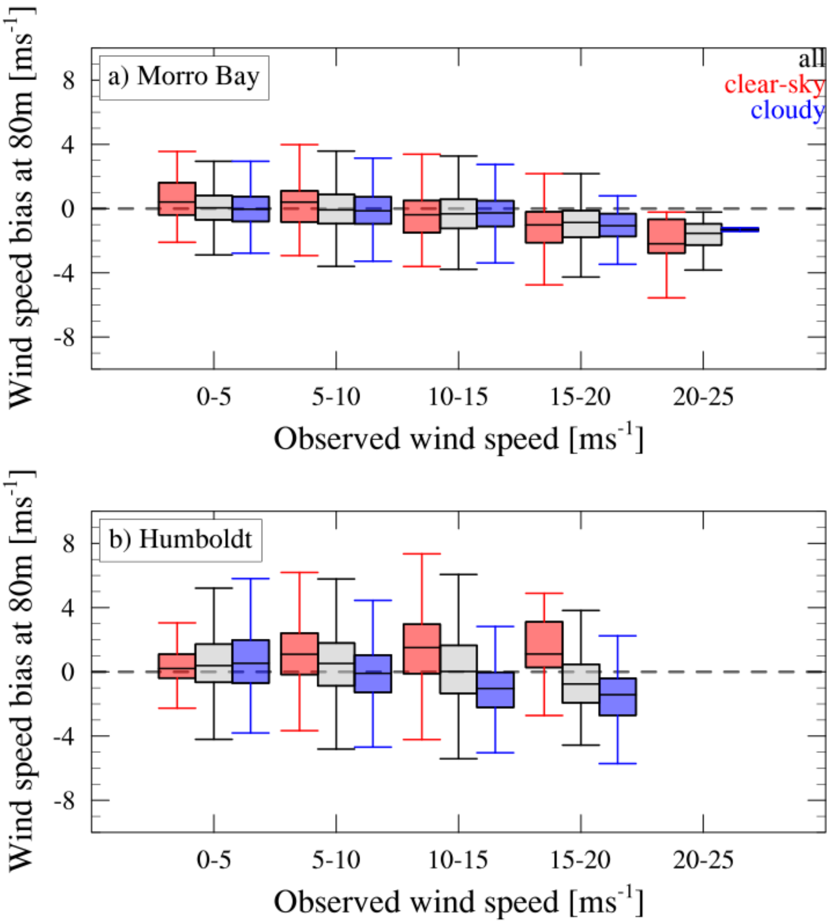

Figure 5 Box whisker plot of wind speed bias at 80 m between HRRR and Lidar (HRRR-Lidar) at various observed wind speed for clear-sky (red), all (grey) and cloudy (blue) conditions at Morro Bay (top) and Humboldt Bay (bottom).

235 We repeated the analysis shown in Fig. 5 for the entire period of available observation data (not shown). For Morro Bay, entire year data is utilized. For Humboldt, the period from December 2020 through May 2021 was excluded due to the unavailability of data. The analysis in the wind speed bias for longer period is consistent with that for warmer months.

https://doi.org/10.5194/wes-2025-108
Preprint. Discussion started: 27 June 2025

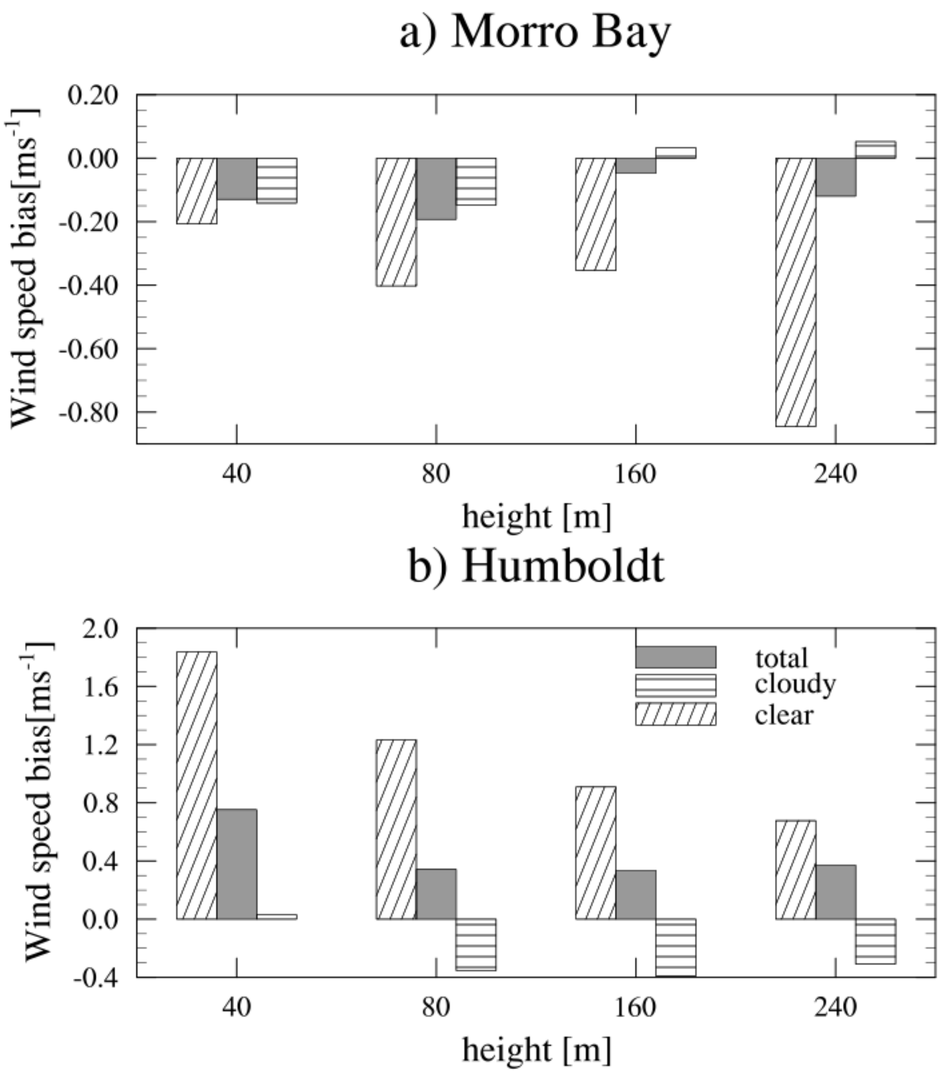

240 **Figure 6 Mean wind speed bias (HRRR - Lidar) for all weather condition in warm season (grey box), clear sky conditions (slanted stripes) and cloudy conditions (horizontal stripes) at various heights below 240m.**

Next, we demonstrate how the mean wind speed bias changes with height (Fig. 6). At Morro Bay, HRRR underestimates the magnitude of low-level wind speed under all weather conditions, with the bias being most pronounced under clear-sky condition. The underestimation of wind speeds by the HRRR model increases with height with underestimation of -0.8 m s^{-1} at 240 m. The HRRR model does simulate winds fairly accurately during cloudy conditions at the Morro Bay.

At Humboldt Bay, HRRR model during clear-sky condition overestimates the rotor layer wind speeds, and underestimates under cloudy condition. The overestimation of winds during clear-sky conditions decreases with height from 40 m to 240 m. Humboldt Bay experiences higher wind shear than Morro Bay. The HRRR model overestimates wind speeds during clear sky conditions at Humboldt Bay and underestimates them at Morro Bay. This suggests that the model has difficulty accurately simulating wind shear in clear sky situations, tending to overestimate winds when shear is strong and underestimate

https://doi.org/10.5194/wes-2025-108
Preprint. Discussion started: 27 June 2025

winds when shear is weak. Although this bias is much smaller during cloudy conditions, the HRRR model still overestimates wind speeds at Morro Bay and underestimates them at Humboldt Bay.

As stated in Optis et al. (2016) and the references therein, similarity-based wind speed profile models produce a large bias under strongly stratified boundary layer. They showed the model bias of wind speed at 4 different heights (40, 80,140, 200 m) using 5 different models under various stable stratification scenario. The model bias grew as the stratification strength increases. Also, the sign of the bias was shown to change under different stratification regime. Although informative, their results cannot be directly extrapolated to an offshore region with high cloudiness such as those studied here. Over land, boundary layer thermodynamic decoupling (stratification) is largely controlled by the presence or absence of surface fluxes as the turbulence is primarily modulated by these fluxes. In contrast, in offshore environments with cloud-topped boundary layer, the turbulence is primarily governed by radiative cooling at the cloud top. As a results, we expect the offshore cloud-topped boundary layers to be coupled at night when the cloud top cooling is strongest and decoupled during the day when the cooling is weakest. In comparison, over land, boundary layers are typically coupled during the daytime when the surface heating is greatest and decoupled at night when the surface heating is minimal.

3.4 Low level wind bias with marine stratocumulus clouds

Cases of warm stratocumulus clouds were identified using the cloud top temperature data from the GOES. The cases were identified from latitude-longitude maps of visible satellite imagery and cloud top temperatures. Three objective criteria, 1) extensive cloud cover for more than 2° (~200 km) in the zonal and meridional direction at the two locations, 2) cloud top temperatures in excess of 0°C, and 3) cloud cover lasting for more than 12 hours were enforced. Most of the cases had duration exceeding multiple days. Some cases had breaks in the cloud for less than 3 hours that got filled and hence were considered part of the same case. Table 3 lists the duration of each identified marine stratocumulus cloud period along with its associated 80-meter wind bias, case-mean observed wind speed, and Pearson correlation coefficient. As previously discussed, hub-height wind speeds and the associated biases at Morro Bay are weaker than those at Humboldt. At both locations, HRRR generally underestimates the hub-height wind speed, except for the case in September at Morro Bay. During that event, the mean wind speed is 4.1 m s^{-1}. During weak wind (0 – 5 m s^{-1}) conditions, HRRR slightly overestimates the hub-height wind speed (Fig. 5). Additionally, the correlation between the timeseries of lidar buoy observations and HRRR wind speed is weaker at Humboldt.

Table 3. List of stratocumulus events and their associated with observed mean wind speed at 80-meter, mean wind bias at 80-meter, and correlation between HRRR and the lidar buoy.

Site	Duration (UTC) YYYYMMDD:HH	bias [m s^{-1}]	Correlation	Observed mean wind speed [m s^{-1}]
Morro Bay	20210510:09 – 20210518:07	-0.26	0.94	5.7
	20210619:02 – 20210709:00	-0.04	0.97	7.8
	20210710:04 – 20210721:02	-0.26	0.94	8.0
	20210802:14 – 20210816:21	-0.27	0.95	7.7

https://doi.org/10.5194/wes-2025-108
Preprint. Discussion started: 27 June 2025

	20210820:03 – 20210827:02	-0.26	0.93	4.3
	20210828:15 – 20210908:07	0.03	0.89	4.6
	20210911:13 – 20210918:16	-0.24	0.96	5.1
	20210922:00 – 20210927:21	0.24	0.89	4.1
	Total hours: 2008	-0.13	0.93	5.9
Humboldt	20210523:22 – 20210525:19	0.03	0.62	5.0
	20210620:20 – 20210707:18	-0.64	0.86	7.4
	20210709:12 – 20210717:23	-0.48	0.83	13.2
	20210724:11 – 20210726:18	-0.57	0.45	12.8
	20210729:15 – 20210805:04	-0.27	0.73	7.2
	Total Hours: 1170	-0.39	0.7	9.12

Figure 7 presents the composite diurnal cycle of cloud top height (a-b), wind speed at 80 meter (c-d) and wind bias (e-f) at both Morro Bay and Humboldt Bay locations during stratocumulus periods listed in Table 3. At Morro Bay, GOES shows a deepening of the cloud layer in the morning while HRRR underestimates this diurnal change. At Humboldt Bay, GOES also indicates a slight deepening of clouds in the morning. These patterns are consistent with the warm season cloud characteristics shown in Fig.2. Wind speed, as shown in Fig 7 (c-d), exihibts a weak diurnal cycle at both locations. At Morro Bay, wind speeds peak in the evening whereas at Humboldt wind speeds increase at night. As indicated in Table 3, wind speeds are generally stronger at Humboldt Bay. The distribution of hub-height wind speed indicates that the bias at both locations is predominantly centered around zero. However, Humboldt exhibits a slightly greater underestimation of wind speed, which aligns with observations presented in Figures 5 and 6. The range of the bias remains between ± 1.5 m s^{-1} at Morro Bay while it exceeds this range at Humboldt. It was shown in Fig. 6 that stronger wind speed induces stronger bias.

https://doi.org/10.5194/wes-2025-108
Preprint. Discussion started: 27 June 2025

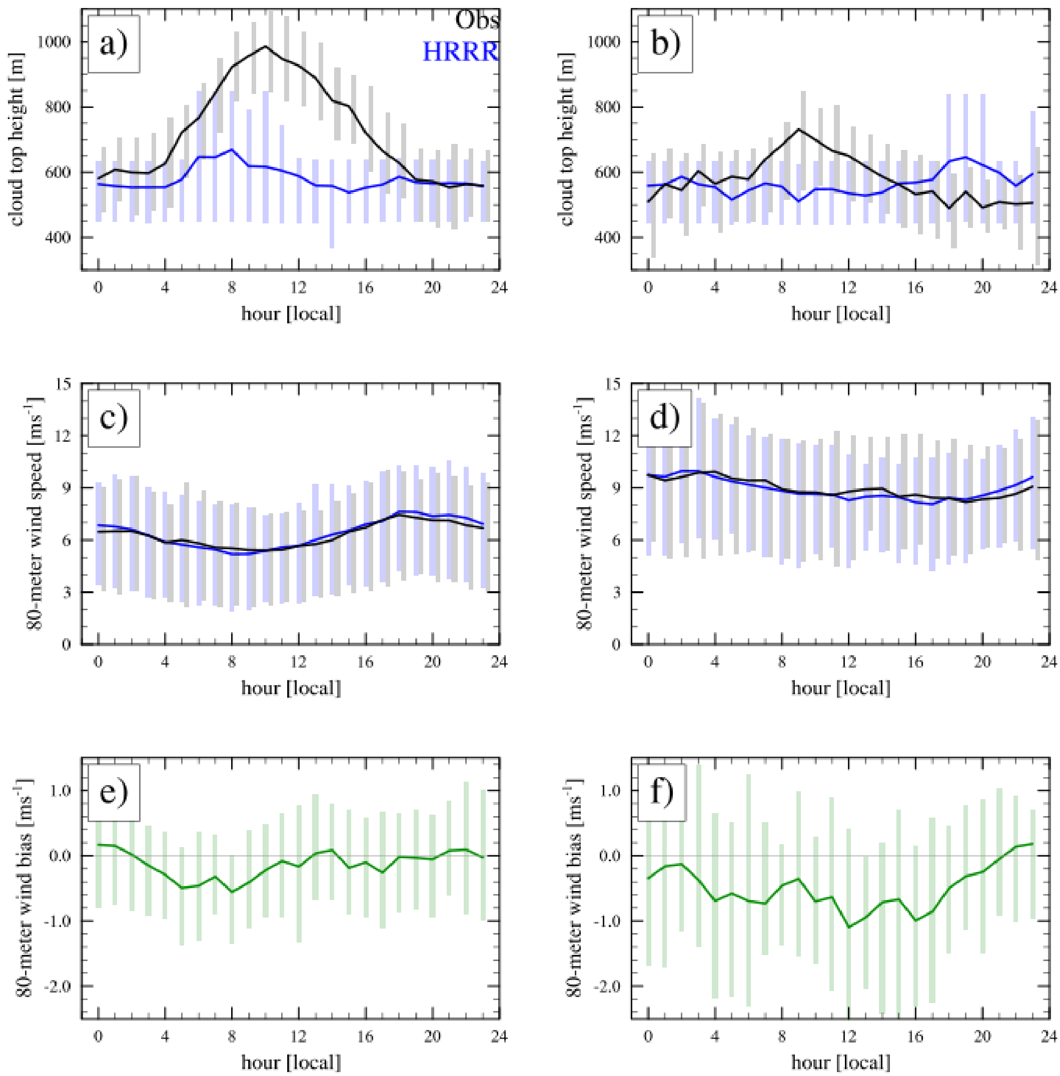

290 **Figure 7 Composite diurnal cycles of a-b) cloud top height, c-d) wind speed at 80-meter height, e-f) wind speed bias between lidar observation and HRRR during the stratocumulus periods listed in Table 3. Left column is from Morro Bay and right column is from Humboldt. Bar represents 25th and 75th percentile while line represents mean. Black lines are from GOES satellite data for cloud top height and lidar data for wind speed, while blue lines represent HRRR results.**

https://doi.org/10.5194/wes-2025-108
Preprint. Discussion started: 27 June 2025

eawe european academy of wind energy
Open Access WIND ENERGY SCIENCE DISCUSSIONS

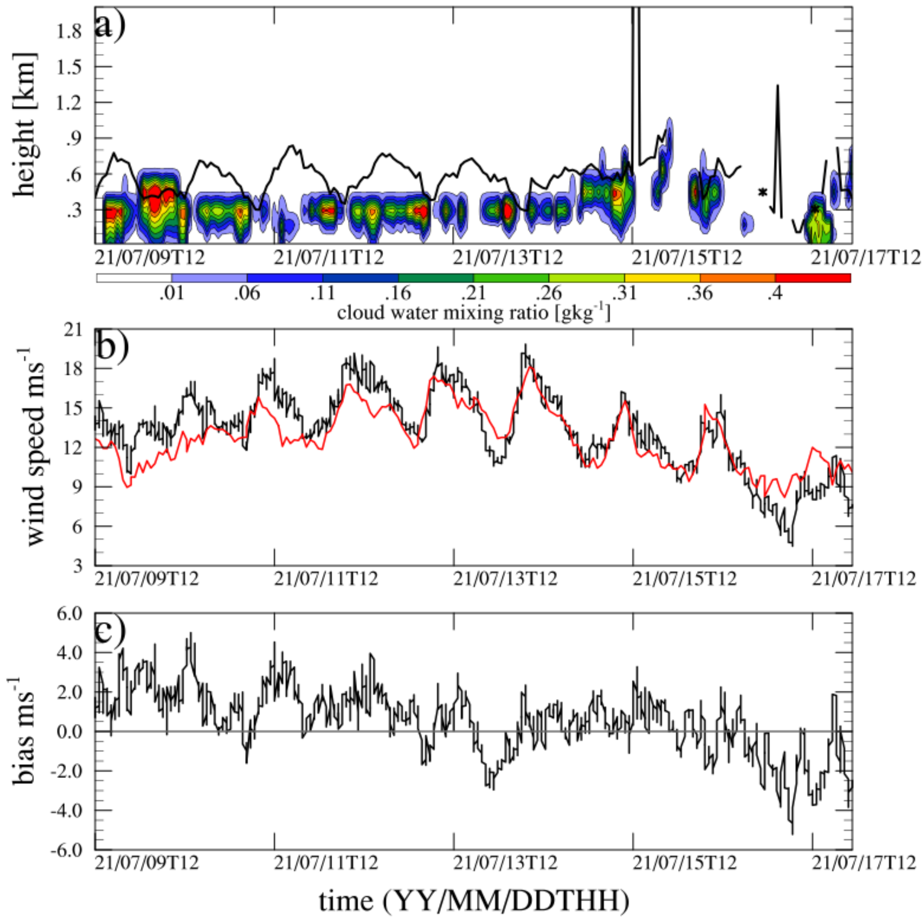

Figure 8 a) timeseries of HRRR simulated cloud water mixing ratio (contour) and GOES reported cloud top height (black line), b) timeseries of wind speed at 80-meter observed by lidar buoy (black) and modeled by HRRR (red), and c) timeseries of wind speed bias (lidar – HRRR) at 80-meter. Location is Humboldt.

In Fig. 8, we closely examine the cloud top height and hub-height wind speed during one of the stratocumulus periods listed in Table 3. Fig. 8 (a) shows the timeseries of the vertical profile of the cloud water mixing ratio simulated by HRRR, alongside the estimated cloud top height by GOES. As shown in section 3.1, HRRR-simulated cloud tops are lower than the GOES-estimated values. While there is no clear indication of a diurnal cycle in cloud top height at Humboldt (Fig. 2b), during this particular period (2021/7/9 – 2021/7/17), GOES cloud top data shows a strong diurnal cycle for the first 5 days. In the observation, clouds are in the form of long-lived sheets while clouds simulated by HRRR is most of the time intermittent as indicated by the gaps in the cloud water mixing ratio. We also compare the 80-meter wind speed between the lidar buoy observation and HRRR simulation. During this stratocumulus period, wind speed consistently exceeds the cut-in speed and occasionally surpassed the rated speed. The observation reveals a very strong diurnal cycle in hub-height wind speed and HRRR reproduces well in terms of amplitude and phase. However, both positive and negative bias exists in HRRR during this period, but the underestimation during the first 4 days outweighs some periods of overestimation (Fig. 8c). The diurnal cycle of the wind speed bias along with the diurnal cycle of the GOES reported cloud top height suggests the bias to be related to the cloud modulated turbulence in the boundary layer.

4. Summary and Conclusion

Marine stratocumulus clouds are shallow and located below the capping marine boundary layer inversion. The radiative cooling at cloud top often generates turbulence mixing downward, which can modulate the PBL turbulence profile (Wood, 2012). Also, the radiative cooling at the cloud top can strengthen the capping inversion, which can generate shear at the inversion layer. This shear is known to initiate atmospheric waves, which can adjust the wind speed and turbulence intensity within the marine boundary layer (Allaerts and Meyers, 2018). Therefore, better understanding the processes within the marine boundary layer bounded by marine stratocumulus clouds is important to better assess and predict wind resources for offshore wind farms in California (Shaw et al., 2022).

There are wind farm lease areas off the coast of Northern and Central California (Musial et al., 2019), where marine stratocumulus clouds are abundant during warmer months (Wood, 2012). In the fall of 2020, two DOE buoys with multiple instruments including Doppler lidar and pyranometer were deployed for about a year to these lease areas (Humboldt and Morro Bay locations) to continuously measure the vertical profile of wind speed below 240 meters and global broadband solar radiation, among others. The presence of this dataset, in combination of GOES satellite date, provides a unique opportunity to assess the HRRR model bias in forecasting the wind speed in rotor-layer relevant heights in terms of cloudiness. The primary findings from this work are as follows.

a) Consistent with previous studies, GOES satellite data indicate that marine stratocumulus clouds are prevalent at both locations during the warmer months. Cloud cover is greater at Morro Bay compared to Humboldt Bay, and Morro Bay also exhibits a more pronounced diurnal cycle in cloud top height. Overall, the HRRR model captures the general cloudiness well but underestimates both the cloud-top heights and the amplitude of the diurnal cycle at both sites, with the underestimation being especially pronounced at Morro Bay.

b) Wind speeds and shear within the rotor layer are stronger at Humboldt Bay than at Morro Bay. At both locations, rotor layer wind speeds and shear are higher on clear-sky days compared to cloudy days. The HRRR model generally reproduces these patterns, although some biases remain.

c) At both locations the HRRR model tends to underestimate the 80-meter wind speed in cloudy condition (with a median bias of -1.5 m s^{-1}), and this negative bias increases with higher wind speeds. Under clear-sky conditions, The wind speed bias is larger with the model overestimating wind speeds at Morro Bay (positive bias) and underestimating them at Humboldt Bay (negative bias).

d) Under cloudy conditions, the mean wind speed bias at different heights (40, 80, 160, and 240 meters) is generally small, close to zero, or shows slight underestimation by the model. Under clear-sky conditions, the opposite bias pattern between Humboldt Bay and Morro Bay remains consistent at all rotor-layer heights.

https://doi.org/10.5194/wes-2025-108
Preprint. Discussion started: 27 June 2025

e) Stratocumulus cloud events at Morro Bay and Humboldt Bay during warmer months were identified by visually inspecting GOES images. Those specific stratocumulus events also reveal that mean wind speed and wind bias are stronger at Humboldt Bay. In both locations, the mean bias is negative.

Due to the shallow depth of marine boundary layer, the top of the surface layer, where Monin-Obukhov (M-O) similarity theory is applicable, could be close to the wind turbine rotor layer. Also, M-O similarity theory is strongly dependent upon the atmospheric stability. Many studies have shown that M-O similarity theory does not work very well above surface layer and under stable stratification. This may explain why the HRRR bias is stronger under clear-sky conditions. The different HRRR bias sign at the two locations under clear-sky condition may be related to the strength of atmospheric stability. Further measurement such as boundary layer thermodynamic profile would be required to verify this theory.

Our analysis uses data only for May through September time-period because that is when marine stratocumulus clouds are most abundant in the region. When we include entire data period including colder months, we get a very similar results as shown in Fig. 6, even though the data period from December through May is missing for Humboldt location: 1) bias is larger under clear-sky conditions than in cloudy condition, 2) bias sign under clear-sky condition is opposite between Humboldt and Morro Bay. Although the fraction of clear-sky days is much lower compared to the cloudiness fraction during warmer months, in colder months, the fraction of clear-sky days increases (not shown). Therefore, it is equally important to improve HRRR model physics to better represent marine boundary layer processes under clear-sky (stable) condition.

Lastly, in this article we characterized the biases in the HRRR model simulated rotor layer winds, and clouds. Broadly the analysis shows the wind speed biases to differ between cloudy and clear-sky conditions, and significant bias in the HRRR simulated cloud fraction and cloud top heights. The turbulence in the cloud-topped boundary layers is modulated by cloud processes, which then in-turn affects the boundary layer thermodynamic stability and winds. To what degree the inaccuracies in representation of clouds affects the representation of winds and vice-versa can only be understood through model simulations. This will be the focus of our work in the near future.

Data availability

Buoy data used in this study are available at https://a2e.energy.gov. All data can be provided by the author upon request.

Author Contribution

All authors contributed to the development of the analysis concept and reviewed the manuscript. JL performed the analysis and wrote the manuscript. AM compiled and provided the GOES and CERES data. LM compiled and provided the buoy data.

Competing Interests

The authors declare that they have no competing interests.

Acknowledgements

Funding for this study was provided by the U.S. Department of Energy (DOE) Office of Energy Efficiency and Renewable Energy, Wind Energy Technologies Office. The views expressed in this article do not necessarily represent those of the DOE or the U.S. Government. VG and AM were supported by the DOE Wind Energy Technologies Office (WETO), Office of Energy Efficiency and Renewable Energy (EERE), under Contract DE-AC02-06CH11357 awarded to Argonne National Laboratory. This work was performed under the auspices of the U.S. Department of Energy by Lawrence Livermore National Laboratory under Contract DE-AC52-07NA27344. LLNL-JRNL-2006801. The language of this manuscript was improved with the assistance of LLNL's LivChat AI service.

References

Allaerts, D., Meyers, J. Gravity Waves and Wind-Farm Efficiency in Neutral and Stable Conditions. Boundary-Layer Meteorol 166, 269–299 (2018). https://doi.org/10.1007/s10546-017-0307-5

Dowell, D. C., and Coauthors, 2022: The High-Resolution Rapid Refresh (HRRR): An Hourly Updating Convection-Allowing Forecast Model. Part I: Motivation and System Description. Wea. Forecasting, 37, 1371–1395, https://doi.org/10.1175/WAF-D-21-0151.1.

Iacobellis, S. F., and D. R. Cayan (2013), The variability of California summertime marine stratus: Impacts on surface air temperatures, J. Geophys. Res. Atmos., 118, 9105–9122, doi:10.1002/jgrd.50652.

Jones, C. R., Bretherton, C. S., and Leon, D.: Coupled vs. decoupled boundary layers in VOCALS-REx, Atmos. Chem. Phys., 11, 7143–7153, https://doi.org/10.5194/acp-11-7143-2011, 2011.

Krishnamurthy, Raghavendra, et al. "Year-long buoy-based observations of the air–sea transition zone off the US west coast." Earth System Science Data (Online), vol. 15, no. 12, Dec. 2023. https://doi.org/10.5194/essd-15-5667-2023

Lin, W., M. Zhang, and N. G. Loeb, 2009: Seasonal Variation of the Physical Properties of Marine Boundary Layer Clouds off the California Coast. J. Climate, 22, 2624–2638, https://doi.org/10.1175/2008JCLI2478.1.

Long, C. N. and T.P. Ackerman, T. P.: Identification of clear skies from broadband pyranometer measurements and calculation of downwelling shortwave cloud effects, J. Geophys. Res.-Atmos., 105, 15609–15626, 2000.

Mahrt, L. Stratified Atmospheric Boundary Layers. Boundary-Layer Meteorology 90, 375–396 (1999). https://doi.org/10.1023/A:1001765727956

Menzel, W. P. and Purdom, J. F. W.: Introducing GOES-I: The First of a New Generation of Geostationary Operational Environmental Satellites, Bulletin of the American Meteorological Society, 75, 757–782, https://doi.org/10.1175/1520-0477(1994)075<0757:IGITFO>2.0.CO;2, 1994.

https://doi.org/10.5194/wes-2025-108
Preprint. Discussion started: 27 June 2025

Minnis, P., Sun-Mack, S., Chen, Y., Chang, F.-L., Yost, C. R., Smith, W. L., Heck, P. W., Arduini, R. F., Bedka, S. T., Yi, Y., Hong, G., Jin, Z., Painemal, D., Palikonda, R., Scarino, B. R., Spangenberg, D. A., Smith, R. A., Trepte, Q. Z., Yang, P., and Xie, Y.: CERES MODIS Cloud Product Retrievals for Edition 4—Part I: Algorithm Changes, IEEE Transactions on Geoscience and Remote Sensing, 59, 2744–2780, https://doi.org/10.1109/TGRS.2020.3008866, 2021.

Musial, Walter D., et al. "2018 Offshore Wind Technologies Market Report." , Sep. 2019. https://doi.org/10.2172/1572771

Optis, M., Monahan, A., and Bosveld, F. C. (2016) Limitations and breakdown of Monin–Obukhov similarity theory for wind profile extrapolation under stable stratification. Wind Energ., 19: 1053–1072. doi: 10.1002/we.1883.

Serpetzoglou, E., B. A. Albrecht, P. Kollias, and C. W. Fairall, 2008: Boundary Layer, Cloud, and Drizzle Variability in the Southeast Pacific Stratocumulus Regime. J. Climate, 21, 6191–6214, https://doi.org/10.1175/2008JCLI2186.1.

Shaw, W. J., Berg, L. K., Debnath, M., Deskos, G., Draxl, C., Ghate, V. P., Hasager, C. B., Kotamarthi, R., Mirocha, J. D., Muradyan, P., Pringle, W. J., Turner, D. D., and Wilczak, J. M.: Scientific challenges to characterizing the wind resource in the marine atmospheric boundary layer, Wind Energ. Sci., 7, 2307–2334, https://doi.org/10.5194/wes-7-2307-2022, 2022.

Sheridan, L. M., Krishnamurthy, R., García Medina, G., Gaudet, B. J., Gustafson Jr., W. I., Mahon, A. M., Shaw, W. J., Newsom, R. K., Pekour, M., and Yang, Z.: Offshore reanalysis wind speed assessment across the wind turbine rotor layer off the United States Pacific coast, Wind Energ. Sci., 7, 2059–2084, https://doi.org/10.5194/wes-7-2059-2022, 2022.

Wharton S., and J. K Lundquist, 2012: Atmospheric stability affects wind turbine power collection. Environ. Res. Lett. 7 014005DOI 10.1088/1748-9326/7/1/014005

Wood, R., 2012: Stratocumulus Clouds. Mon. Wea. Rev., 140, 2373–2423, https://doi.org/10.1175/MWR-D-11-00121.1.

Zamora Zapata, M., Heus, T., & Kleissl, J. (2021). Effects of surface and top wind shear on the spatial organization of marine Stratocumulus-topped boundary layers. Journal of Geophysical Research: Atmospheres, 126, e2020JD034162. https://doi.org/10.1029/2020JD034162